Metabolic cleavage and translocation efficiency of selected cell penetrating peptides

A comparative study with epithelial cell cultures

Author(s):
Foerg, Christina; Weller, Kathrin M.; Rechsteiner, Helene; Nielsen, Hanne M.; Fernandez-Carneado, Jimena; Brunisholz, Rene; Giralt, Ernest; Merkle, Hans P.

Research Article

Metabolic Cleavage and Translocation Efficiency of Selected Cell Penetrating Peptides: A Comparative Study with Epithelial Cell Cultures

Christina Foerg,[1,6] Kathrin M. Weller,[1] Helene Rechsteiner,[2] Hanne M. Nielsen,[3] Jimena Fernández-Carneado,[4] René Brunisholz,[2] Ernest Giralt,[4,5] and Hans P. Merkle[1]

Abstract. We investigated the metabolic stability of four cell penetrating peptides (CPPs), namely SAP, hCT(9-32)-br, [Pα] and [Pβ], when in contact with either subconfluent HeLa, confluent MDCK or Calu-3 epithelial cell cultures. Additionally, through analysis of their cellular translocation efficiency, we evaluated possible relations between metabolic stability and translocation efficiency. Metabolic degradation kinetics and resulting metabolites were assessed using RP-HPLC and MALDI-TOF mass spectrometry. Translocation efficiencies were determined using fluorescence-activated cell sorting (FACS) and confocal laser scanning microscopy (CLSM). Between HeLa, MDCK and Calu-3 we found the levels of proteolytic activities to be highly variable. However, for each peptide, the individual degradation patterns were quite similar. The metabolic stability of the investigated CPPs was in the order of CF-SAP = CF-hCT(9-32)-br > [Pβ]−IAF > [Pα] and we identified specific cleavage sites for each of the four peptides. Throughout, we observed higher translocation efficiencies into HeLa cells as compared to MDCK and Calu-3, corresponding to the lower state of differentiation of HeLa cell cultures. No direct relation between metabolic stability and translocation efficiency was found, indicating that metabolic stability in general is not a main limiting factor for efficient cellular translocation. Nevertheless, translocation of individual CPPs may be improved by structural modifications aiming at increased metabolic stability.

KEY WORDS: cell penetrating peptides; cellular translocation; epithelial cell cultures; metabolic cleavage; metabolism kinetics.

INTRODUCTION

The appealing prospects of peptide, protein and nucleic acid therapeutics has made the delivery of large and hydrophilic molecules across the plasma membrane into the cytoplasm and to cellular organelles a vital issue for current and future drug development. Owing to the barrier properties of the plasma membrane, the cellular uptake of such biopolymers is inherently poor, necessitating the development of efficient delivery vectors. Hence, chemical coupling or physical assembly of biopolymers of poor cellular accessibility with so-called cell penetrating peptides (CPPs) has turned into a prime topic in the biomedical engineering of delivery

Both Christina Foerg and Kathrin M. Weller contributed equally to the present work.

[1] Institute of Pharmaceutical Sciences, ETH Zurich, Hönggerberg Campus, Wolfgang-Pauli-Strasse 10, CH-8093, Zurich, Switzerland.
[2] Functional Genomics Center Zurich, UNI, Irchel, Switzerland.
[3] Department of Pharmaceutics and Analytical Chemistry, The Danish University of Pharmaceutical Sciences, Copenhagen, Denmark.
[4] Institut de Recerca Biomèdica de Barcelona, Parc Científic de Barcelona, Barcelona, Spain.
[5] Departament de Química Orgànica, Universitat de Barcelona, Barcelona, Spain.
[6] To whom correspondence should be addressed. (e-mail: christina. foerg@pharma.ethz.ch)

systems that are hoped to mediate the non-invasive import of such therapeutics into cells (1–8).

A major obstacle to CPP mediated drug delivery consists in the often rapid metabolic clearance of the peptides when in contact or passing the enzymatic barriers of epithelia and endothelia (9). Prior to release of the cargo at its destination, cell penetrating peptides should be sufficiently stable when carrying the chemically ligated or physically complexed cargo across the barrier. Nevertheless, information on the enzymatic stability and degradation of CPP is rare (10–14). For instance, the stability of pVEC, a CPP derived from murine vascular endothelial cadherin, was previously assessed by Langel and coworkers (11,12). pVEC was rapidly degraded when incubated with human aorta endothelial cells and murine A9 fibroblasts. By contrast, when the ʟ-amino-acid residues of its sequence were replaced by their non-natural ᴅ-counterparts, pVEC was no longer susceptible to degradation, without losing its translocating properties (12). Another related study focused on the metabolic stability of the transportan analogue transportan 10, and penetratin, revealing transportan 10 as the most, and penetratin as the least, metabolically stable peptide among the three CPPs (14). Moreover, we analyzed the metabolic degradation kinetics and the cleavage patterns of selected CPPs, namely human calcitonin (hCT) derived peptides, Tat(47-57) and penetratin(43-58) by incubation with three epithelial models, MDCK, Calu-3 and TR 146 cell layers (13). The proteolytic activities among the different

epithelial models and the CPPs were highly variable. Yet the individual patterns between the three models for the metabolic degradation of each peptide were strikingly similar.

In the present study, we aimed to explore a potential relationship between the metabolic stability of CPPs and their translocation capacity. To this end we focused on (1) the metabolic degradation kinetics and cleavage patterns of four oligocationic CPPs when in contact with epithelial cell cultures, and on (2) the efficiency of their cellular uptake. We used cultures from three epithelial cell lines, HeLa (15), MDCK (16) and Calu-3 cells (17). The sequences of the four investigated CPPs are listed in Table I: The first one is the carboxyfluorescein (CF) labeled linear proline-rich sweet arrow peptide CF-SAP, a linear trimer of repetitive VRLPPP domains, and designed as an amphipathic version of a polyproline sequence related to γ-zein, a storage protein of maize (18–20). Another one is a branched modification of the previously reported linear human calcitonin (hCT) derived CF-hCT(9-32) (21). It is denoted as CF-hCT(9-32)-br (22) and carries the oligocationic, SV40 large T antigen in the form of a side-branch to the main peptide chain. Previous studies revealed that both CF-SAP and CF-hCT(9-32)-br were non-toxic even in higher concentrations, and readily translocated into HeLa cells as triggered by interaction with the negatively charged extracellular matrix, followed by lipid raft-mediated endocytosis (23). In addition we investigated two members of the so called MPG family: the first, [Pβ]-IAF, carrying the C-terminal iodoacetamido-fluorescein (IAF) fluorescence marker, combines the hydrophobic fusion peptide of HIV-1 gp41 and the oligocationic sequence of SV40 large T antigen. The peptide was originally synthesized by Vidal *et al.* (24) and has been previously demonstrated to deliver oligonucleotides into cultured cells (25). To directly monitor its cellular uptake, the peptide was C-terminally labeled with IAF. The second member of the MPG family, [Pα] has been developed through amino acid modifications of [Pβ] in five positions, aiming at an α-helical structure (20,26). Because of severe solubility problems with fluorescently labeled [Pα]-IAF, we studied the metabolism of the non-labeled peptide only. Deshayes *et al.*(26) previously reported about the high affinity of [Pα] for membranes and its secondary structure required for uptake. The near negligible toxicity of [Pα] and [Pβ] has been reported by Fernandez *et al.* (20).

CF-SAP and CF-hCT(9-32)-br demonstrated marked metabolic stability under all experimental conditions, whereas, in contrast, [Pα] and [Pβ]-IAF showed drastic enzymatic degradation, and decomposed quickly even when incubated in serum free medium. Moreover, we were able to identify specific cleavage sites for each of the four peptides. Emphasizing the relevance of the chosen cellular models, we found the uptake

efficiencies of all four CPPs to be strongly cell line dependent. Interestingly, despite their high enzymatic stability, CF-SAP and CF-hCT(9-32)-br showed only low extents of translocation into well differentiated cell layers. This excludes enzymatic degradation to represent a main factor that limits cellular translocation. Nevertheless, with respect to [Pα] and [Pβ]-IAF improved stability through structure modification cannot be excluded to further enhance their performance as CPPs.

MATERIALS AND METHODS

Materials. HeLa and Calu-3 cells were obtained from American Type Culture Collection ATCC (Rockville, MD, USA). The MDCK cell line (low resistance, type II) was a gift from the Biopharmacy group of ETH Zurich (Switzerland) (27). Cell culture media, trypsin-EDTA, penicillin, streptomycin and Hanks Balanced Salt Solution (HBSS) were from Gibco (Paisley, USA). Fetal calf serum (FCS) was either obtained from HyClone (Logan, Utah, USA) or from Fisher Scientific (Wohlen; Switzerland) and Hoechst 33342 from Molecular Probes (Leiden, Netherlands). Cell culturing flasks 25 cm² were from TPP (Trasadingen, Switzerland). Cell culture inserts (polyethylene terephthalate (PET), 0.4 μm pore size, 1.6×10^6 pores per square centimeter, 0.9 cm² growth area), companion 12 well plates, 24 well plates and 5 ml polypropylene round-bottom tubes (FACS tubes) were purchased from Falcon (Becton Dickinson Labware, Franklin Lakes, NJ, USA). Ninety-six well plates and 8 well glass chamber slides were obtained from Nunc (Roskilde, Denmark). Aqueous 0.4% Trypan blue solution with 0.81% sodium chloride and 0.06% potassium phosphate, DMSO and 5(6)-carboxyfluorescein (CF) were purchased from Fluka (Buchs, Switzerland), and Bradford reagent from Sigma (St. Louis, MO, USA). α-cyano-4-hydroxy-cinnamic acid was obtained from Agilent Technologies (Burnsville, Minnesota, USA), ZipTip from Millipore (Bedford, MA, USA).

Peptides. The investigated CPPs are listed in Table I. N-terminally CF-labeled sweet arrow peptide, CF-SAP, was synthesised by solid-phase peptide synthesis on a 2-chlorotrityl resin following the 9-fluorenyl methoxy carbonyl/*tert*-butyl strategy prior to labeling with 5(6)-carboxyfluorescein (19). The branched human calcitonin (hCT) derived CPP, N-terminally labeled with 5(6)-carboxyfluorescein (CF), CF-hCT(9-32)-br, was synthesized by the peptide synthesis unit of the University of Barcelona (Spain). CF-hCT(9-32)-br derives from the linear hCT(9-32) CPP (13,21) and was equipped with the oligocationic SV40 large T antigen in the side chain of K_{18} (22). [Pα] and C-terminally 5-(iodoaceta-

Table I. Amino Acid Sequences and Molecular Weights of the Investigated CF and IAF Modified CPPs

Name	Sequence[a]	MW[b] (Da)
CF-SAP	CF-V*R*LPPP-V*R*LPPP-V*R*LPPP	2,356
CF-hCT(9-32)-br	CF-LGTYTQDFNKFHTFPQTAIGVGAP-NH2 | AFGVGPDEV*KRKKK*P-NH2	4,606
[Pα]	Ac-GALFLAFLAAALSLMGL-WSQ-P*KKKRK*V-Cya	3,047
[Pα]-IAF	Ac-GALFLAFLAAALSLMGL-WSQ-P*KKKRK*V-Cya-IAF	3,434
[Pβ]-IAF	Ac-GALFLGFLGAAGSTMGA-WSQ-P*KKKRK*V-Cya-IAF	3,296

[a] Basic aa are indicated in italics
[b] Calculated molecular weight of the peptides

mido)-fluorescein (IAF) labeled [Pα], [Pα]-IAF, as well as C-terminally IAF labeled [Pβ] [Pβ]-IAF, were obtained from NMI TT GmbH (Reutlingen, Germany). Common structural elements of [Pα], [Pα]-IAF and [Pβ]-IAF are a non-polar HIV derived sequence, HIV-1 gp41, and the polar, oligocationic sequence of SV40 large T antigen, KKKRKV, connected via a self-fluorescent WSQP spacer (20,24,25,28). Owing to the poor aqueous solubility of the IAF-labeled [Pα]-IAF, we analyzed its metabolism kinetics with unlabeled [Pα] which was sufficiently soluble. However, for FACS and CLSM, which required more sensitive fluorescence detection, we used [Pα]-IAF expecting translocation to occur with dissolved peptide only.

Cell Culture. Cells were cultured under standard conditions in 25 cm^2 culture flasks at 37°C and 5% CO_2. HeLa and Calu-3 cells were maintained in Dulbecco's modified Eagle medium (DMEM), MDCK cells in minimum essential medium with Earl' salts (MEM). Media contained 10% heat-inactivated FCS and 1% penicillin/streptomycin. Each cell line was used within a range of ten consecutive passage numbers (HeLa: 9–15; MDCK: 225–235; Calu-3: 36–42).

Confocal Laser Scanning Microscopy (CLSM) of Cellular Uptake. We estimated the cellular uptake of fluorescently labeled CPPs by CLSM. HeLa cells were seeded onto eight well glass chamber slides at a density of 40,000 cells per square centimeter and were used 1 day after seeding as exponentially growing, subconfluent cells. MDCK and Calu-3 cells were seeded at a constant density of 20,000 or 50,000 cells per square centimeter, respectively and were used at day 10 or 16, respectively, as fully confluent monolayers. For uptake experiments, cells were incubated in 150 μl serum free medium containing fluorescently labeled CPP or unconjugated fluorophore at a concentration of 20 μM for 2 h under standard cell culture conditions. We used 2 mM stock solutions of CPP or unconjugated fluorophore, respectively, in DMSO that were further diluted with serum free medium to obtain a final concentration of 20 μM. For the last 30 min of incubation, Hoechst 33342 was added for nuclear staining at a final concentration of 1 μg/ml. Prior to microscopy, cells were rinsed three times with HBSS buffer and overlaid with HBSS buffer. To avoid fixation artefacts, we abstained from any fixation of the samples (29) Additionally, to avoid misinterpretation due to extracellular fluorescence bound to cell membranes or working materials, half of the volume was replaced with aqueous 0.4% Trypan blue solution. Trypan blue is unable to translocate intact cell membranes which makes it a selective quencher for extracellularly bound fluorescence (30–32). Cells were then scanned using a Zeiss CLSM 410 inverted microscope. Image processing was performed with Imaris, a 3D multi-channel image processing software for confocal microscope images (Bitplane, Zurich, Switzerland).

As controls, HeLa, MDCK or Calu-3 cells were incubated with peptide-free medium or with the fluorescence marker carboxyfluorescein alone (data not shown).

Quantification of CPP Translocation by Fluorescence Activated Cell Sorting (FACS). We used FACS analysis to quantify the translocation of fluorescently labeled CPPs. As with CLSM, HeLa cells were seeded onto 24 well plates at a density of 40,000 cells per square centimeter and were used 1 day after seeding as exponentially growing cells. MDCK and Calu-3 cells were seeded at a constant density of 20,000 or 50,000 cells per square centimeter, respectively, and were used at day 10 or 16, respectively, as fully confluent monolayers. For uptake experiments, cells were incubated in 250 μl serum free medium containing fluorescently labeled CPP or unconjugated fluorophore at a concentration of 20 μM for 2 h under standard cell culture conditions. Prior to dilution with serum free medium, 2 mM stock solutions of the respective CPP or unconjugated dye in DMSO were prepared. After incubation, all cells were extensively washed with PBS buffer. To cleave adhering CPP from the cell membranes and to detach the cells from the well plates, HeLa cells were trypsinized for 5 min, MDCK and Calu-3 cells for 15 min, as adapted from the literature (29,33). Cells were then transferred into FACS tubes and washed once with PBS prior to further analysis. Half of the volume was replaced with aqueous 0.4% Trypan blue solution to quench extracellular CPPs (34,35). Cells were analyzed by FACS on a FacsCalibur (BectonDickinson, Franklin Lakes, NJ) within 1 h after trypsinization. A total of 8,000 gated cells per sample was counted. Data were analyzed using Cytomation Summit software (Cytomation Inc., Fort Collins, USA). As controls, HeLa, MDCK or Calu-3 cells were incubated with peptide-free medium or with the fluorescence marker carboxyfluorescein alone (data not shown).

CPP Stability in Serum Free Medium. We used 2 mM stock solutions of CPPs or unconjugated fluorophore, respectively, in DMSO that were further diluted with serum free medium to a final concentration of 20 μM. Tightly closed and protected against light, the tubes were incubated for 21 days at 37°C under mechanical shaking (150 min^{-1}). Every second or third day, a sample of 50 μl was withdrawn from each tube and analyzed by RP-HPLC and MALDI-TOF MS.

Metabolism Kinetics of CPP in Contact With Cell Cultures— RP-HPLC. HeLa and MDCK cells were seeded and cultivated as described above for FACS studies. Calu-3 cells were plated onto filter supports at a constant density of 100,000 cells per square centimeter. After the cells had attached to the filter overnight, the medium was removed from the apical compartment to allow the monolayer to grow at the air interface. Prior to metabolic degradation, Calu-3 cells were equilibrated for 30 min at 37°C with serum free medium in order to adjust the apical side to the experimental conditions. Twenty micromole of each of the investigated CPPs were dissolved in the respective medium and added to the apical side. Mechanical shaking at 150 min^{-1} was applied to minimize the thickness of the aqueous boundary layer. Samples of 50 μl were taken from the apical compartment after 1 and 30 min, and 1, 2, 3, 4, 6 and 8 h incubation for HeLa and MDCK cells, and after 1, 15, 30 and 45 min, and 1, 2, 3, and 8 h incubation for Calu-3 monolayers. As controls, HeLa, MDCK or Calu-3 cells were incubated with peptide-free medium and samples were taken as described above. Immediately after taking the samples, 2.5 μl acetic acid (3.7 M) was added in order to stop enzyme activity (36). Determination of the respective half-lives was by RP-HPLC. Throughout, we used a Merck-Hitachi RP-HPLC (VWR International, Dietikon, Switzerland). In order to improve analytical sensitivity, degradation of CF-SAP, CF-hCT(9-32)-br and [Pβ]-IAF was monitored by fluorescence detection of the labels. Accordingly, detection was limited to intact fluorescently labeled peptides and their N- or C-terminal

metabolites carrying the N- or C-terminally ligated fluorophore, respectively. Fluorescence was excited at 492 nm and detected at 517 nm. Due to the insufficient solubility of labeled [Pα]-IAF, unlabeled [Pα] was used for analysis of metabolism kinetics as the experimental setting did not necessarily require IAF fluorescence detection. Therefore, we performed UV detection at 216 nm, and fluorescence detection of tryptophane at 283 nm for excitation and 350 nm for emission.

RP-HPLC of CPPs was performed as follows: For CF-SAP we used a linear gradient mobile phase starting at 25% solvent A consisting of AcCN/TFA, 99.9:0.1 (*v/v*) to 25% solvent B (water/TFA, 99.9:0.1) over 40 min. For CF-hCT(9-32)-br the linear gradient mobile phase was 30% solvent A to 20% solvent B over 20 min. In case of [Pα] the linear gradient mobile phase was 50% solvent A to 0% solvent B over 25 min, and for [Pβ]-IAF 20% solvent A to 20% solvent B over 40 min. An analytical RP-18 column with 250×4.6 mm, particle size 5 μm, pore diameter 300 Å from Vydac (Hesparia, CA, USA) was applied. The flow rate was 1 ml/min. Peptide concentrations were calculated from the area under the curve. The data were empirically evaluated according to pseudo first-order kinetics.

To account for the difference in the cross sectional area of the cell culture inserts—2 cm^2 with HeLa and MDCK cells *versus* 0.9 cm^2 with Calu-3 cells—the experimental half-lives were normalized to 1 cm^2. This approximation was strictly limited to the assumption of linear kinetics for the studied concentration range and excluded any enzyme saturation. Also all effects of diffusion kinetics were neglected. All experiments were run in triplicate.

Analysis of Cell Line Specific Protein Content and Cell Density. The content of protein per well was assessed for each cell line. For this purpose, seeding conditions of all cell models such as density and time of growth were kept as described for the FACS experiments. As described by the manufacturer, cells were lysed and analyzed using a Bradford assay in a 96 well plate by measuring the absorption at 595 nm with a ThermoMax microplate reader (Molecular Device, Sunnyvale, CA, USA). Standard curves were established using BSA dissolved in HBSS. Results were normalized to milligrams protein per square centimeter cell culture surface.

Cells were counted using a haemocytometer (Assistent, Sondheim/Rhön, Germany), and the results were converted into number of cells per square centimeter cell culture surface. All experiments were performed in triplicate.

Identification of Metabolites Using MALDI-TOF MS. Metabolites emerging from the degradation of the investigated CPPs in contact with the cell cultures were identified by matrix assisted laser desorption ionization time of flight mass spectroscopy (MALDI-TOF MS) analysis. Samples were directly taken from cell culture incubates. For this purpose, 1 μl samples containing CPP and/or metabolites thereof were mixed with 2 μl of a saturated matrix solution of α-cyano-4-hydroxy-cinnamic acid. Of this solution, 0.7 μl was applied to the target plate, allowed to crystallize, and dedusted. CF-SAP, [Pα], and [Pβ]-IAF were analyzed in reflectron mode, CF-hCT(9-32)-br in linear mode. Mass acquisition ranged from 750 to 6,000 Da. External calibration was performed with a peptide mix ranging between 900 and 1,700 Da. All experiments were performed in triplicate. For each of the CPPs in contact with either one of the cell models, one sample per time point was pre-treated in order

to desalt the sample and increase the detection limit and accuracy using ZipTip according to the manufacturer's instructions. Analysis was performed on a MALDI-TOF mass spectrometer 4700 Proteomics analyzer type AB347000084 Applied Biosystems (Foster City, USA).

RESULTS

Cell Line Dependent Translocation. To investigate a potential relation between metabolic stability and translocation efficiency of the CPPs in three epithelial cell lines, we first determined their efficiency of translocation. HeLa, MDCK and Calu-3 cell cultures were exposed to either one of the four cationic CPPs: CF-SAP, CF-hCT(9-32)-br, [Pα]-IAF and [Pβ]-IAF. Owing to their strong cationic charge, the CPPs closely sticked to cell membranes rendering direct interpretation of CLSM data difficult (Fig. 1b). As shown in Fig. 1c, Trypan blue efficiently quenched extracellular fluorescence. Therefore, all CLSM studies were strictly performed under Trypan blue quenching.

After incubation for 2 h at 37°C, there was ready cellular uptake of all four CPPs in non-confluent, proliferating HeLa cells (Fig. 2). As shown in Fig. 2, significantly lower amounts of each of the four CPPs was taken up by the confluent MDCK layers. CF-SAP and CF-hCT(9-32)-br mainly accumulated in the paracellular space between the cells. Obviously, paracellular fluorescence was not accessible to Trypan blue quenching. In the confluent Calu-3 model, none of the four
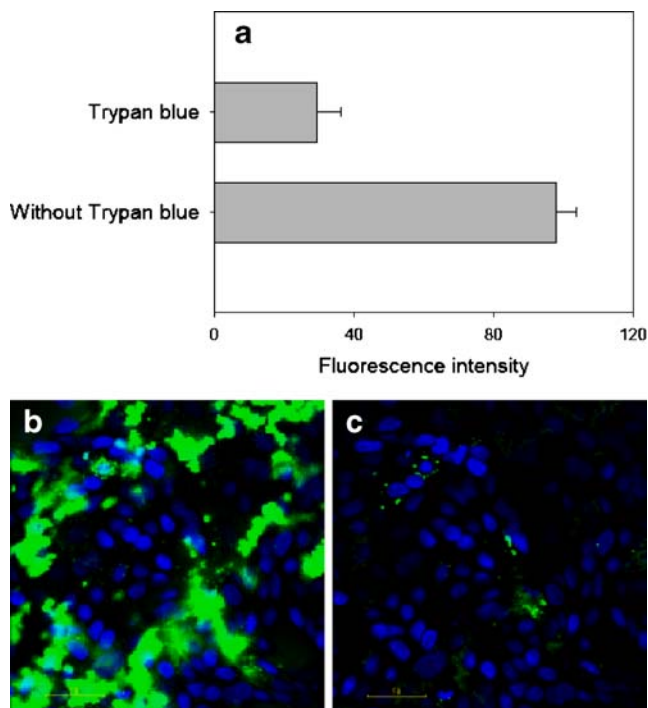

Fig. 1. Quenching effect through the addition of Trypan blue. MDCK cells were incubated with [Pβ]-IAF in the absence or in the presence of Trypan blue and analyzed by FACS (**a**) and CLSM in the absence (**b**) or in the presence (**c**) of Trypan blue. Cell nuclei (*in blue*) were stained with Hoechst 33342. CPPs are displayed in *green*. *Bar*=50 μm

investigated CPPs showed any relevant translocation or accumulated in the paracellular space. Non-treated cells and cells incubated with the fluorescence marker carboxyfluorescein alone did not show significant intracellular or paracellular fluorescence (data not shown).

Quantification of CPP Translocation by FACS Analysis. For confirmation and quantification of our CLSM findings, we also tested the extents of translocation by FACS analysis (Fig. 3). Figure 3a compares the uptake of CF-SAP in the three different cell models. Similar to CLSM data, confluent
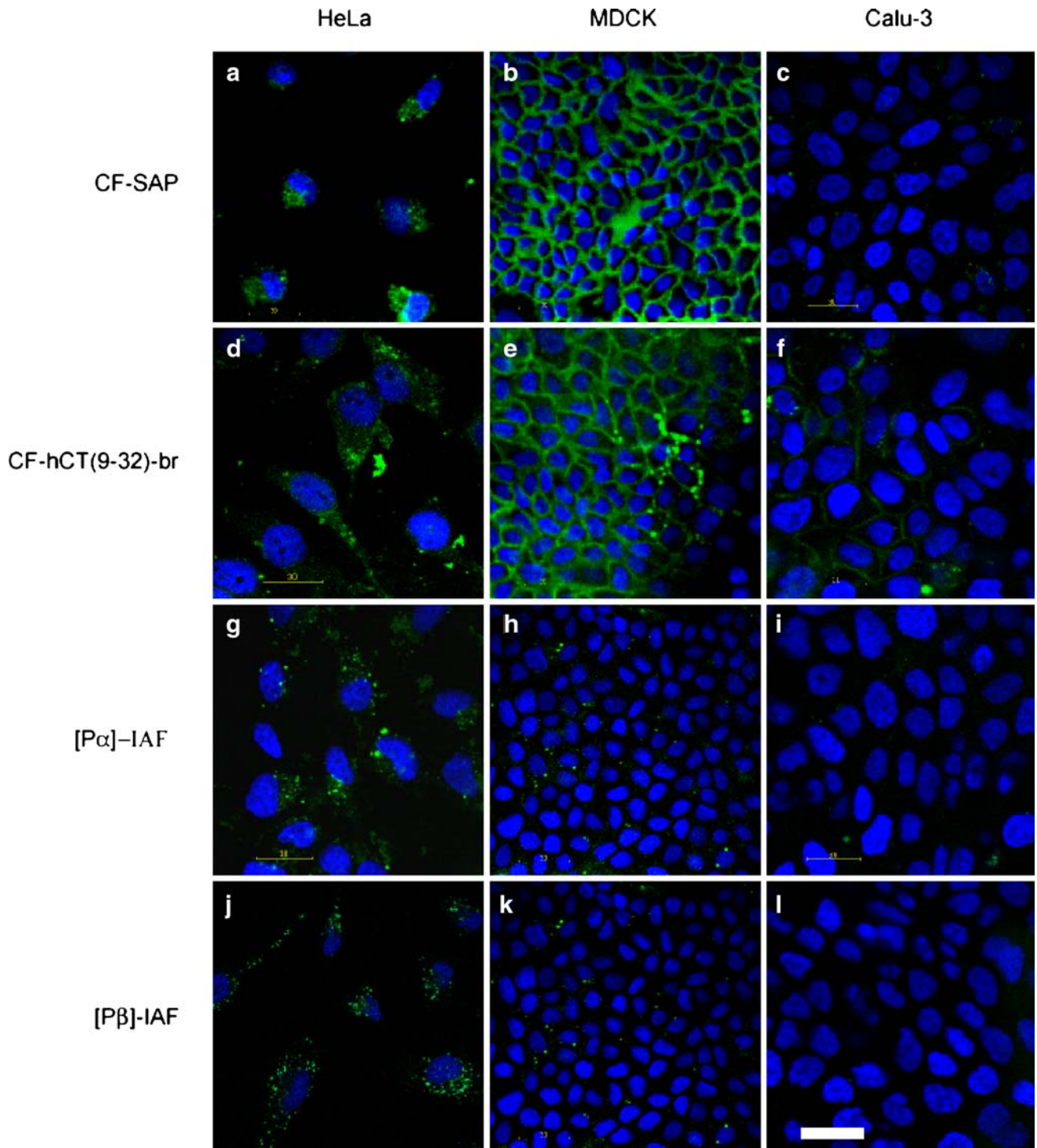
Fig. 2. Translocation of CPPs in epithelial cell models. Each of the cell models, HeLa (**a**, **d**, **g**, **j**), MDCK (**b**, **e**, **h**, **k**) and Calu-3 (**c**, **f**, **i**, **l**), was incubated for 2 h with the investigated CPPs: CF-SAP (**a**, **b**, **c**), CF-hCT(9-32)-br (**d**, **e**, **f**), [Pα]-IAF (**g**, **h**, **i**) or [Pβ]-IAF (**j**, **k**, **l**) and cells were observed by CLSM. Cell nuclei (displayed in *blue*) were stained with Hoechst 33342. *Bar*=50 μm. Translocation of CF-SAP (**a**) and CF-hCT(9-32)-br (**d**) in HeLa was previously reported (23) but added for completeness
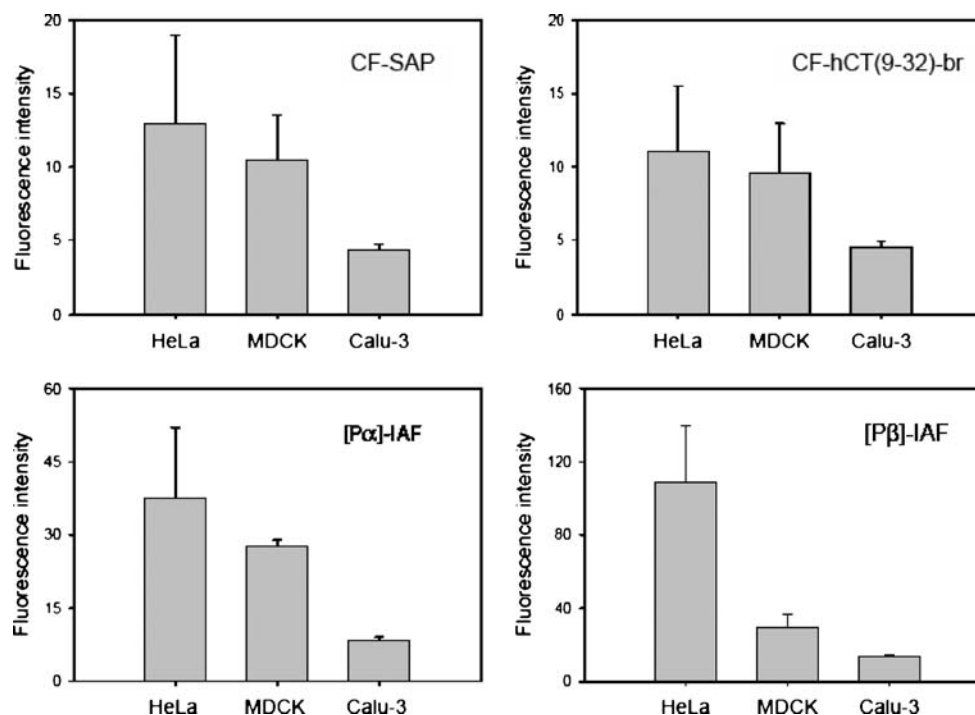
Fig. 3. Quantification of translocated CPPs in cell models. Each cell model, HeLa, MDCK and Calu-3, was incubated for 2 h with the investigated CPPs: CF-SAP, CF-hCT(9-32)-br, [Pα]-IAF or [Pβ]-IAF and analyzed by FACS analysis. Mean cell fluorescence±SD ($n=3$)

Calu-3 cells showed rather low extents of translocation. Higher extents were found in confluent MDCK layers, and highest in non-confluent, proliferating HeLa cells. The cell model-dependent drop in translocation was the same for all investigated CPPs (Fig. 2a–d). Throughout, HeLa cells featured the highest extents of translocation, whereas the well differentiated and polarized MDCK and Calu-3 layers showed lower or no relevant uptake. Non-treated cells and cells incubated with free fluorophore were used as negative controls. There was no uptake whatsoever into untreated cells and cells treated with the fluorophore alone. In all studies, we used Trypan blue quenching to exclude adherent extracellular fluorescence. As shown in Fig. 1a, a drastic drop in fluorescence intensity occurred when Trypan blue was added to the cell suspension prior to FACS analysis.

Peptide Stability in Serum Free Medium. To explore the chemical stability of the four CPPs over the duration of the translocation experiments, we performed exploratory chemical stability studies of all investigated CPPs in the respective medium without serum. CF-SAP and CF-hCT(9-32)-br showed good stability over 7 days in serum free medium. After the same period of time, however, only 70% of [Pβ]-IAF and strikingly low 18% of [Pα] were detected (data not shown). Thus, with the exception of [Pα], all compounds demonstrated reasonable or good chemical stability for metabolism studies of up to 8 h.

Protein Content and Cell Density of Cell Models. As shown in Table II, the protein contents of the employed cell models ranged from 1.55±0.13 mg/cm^2 for HeLa cells to 6.17± 2.2 mg/cm^2 for Calu-3 cells. The cell number per square centimeter was found to be highest for MDCK cells with a cell density of 520,000 cells per square centimeter and lowest

for HeLa cells with a cell density of 47,083 cells per square centimeter.

Kinetics of Metabolic Degradation of CPPs in Contact with Epithelial Cell Cultures. To analyze the susceptibility of the four CPPs to metabolic degradation as well as to evaluate contrasts in metabolism kinetics between the investigated cell lines, we determined the metabolic degradation of CF-SAP, CF-hCT(9-32)-br, [Pα] and [Pβ]-IAF upon incubation with HeLa cells, and MDCK and Calu-3 cell layers. Because of severe solubility problems with fluorescently labeled [Pα] we used its unlabeled form only. The obtained degradation profiles of the CPPs were evaluated according to pseudo first-order degradation kinetics, with the semilogarithmic ln *c versus t* graphs showing a linear dependence. The results were based on three experiments utilizing cells of the same passage for each combination of peptide and cell line. The half lives are given in Table III. During the investigated time interval of 8 h, CF-SAP and CF-hCT(9-32)-br were essentially stable in all cell models. Much shorter half-lives were observed for

Table II. Protein contents and Cell Densities in HeLa, MDCK and Calu-3 Cell Models

Cell line	Protein content (mg/cm^2)	Cell number per square centimeter
HeLa	1.55±0.13	47,083±6,166
MDCK	3.03±0.64	520,000±36,055
Calu-3	6.17±2.20	353,333±32,145

Measurements performed on cells seeded and cultured as described for use in FACS and CLSM experiments. Mean values±SD ($n=3$) are given.

Table III. Metabolic Degradation of CF-SAP, CF-hCT(9-32)-br, [Pα] and [Pβ]-IAF on Different Cell Models Represented as Normalized Half-Lives

Peptides	Half-life (h)		
	HeLa	MDCK	Calu-3
CF-SAP	Stable	Stable	Stable
CF-hCT(9-32)-br	Stable	Stable	Stable
[Pα]	0.94±0.28	0.98±0.08	0.43±0.05
[Pβ]-IAF	5.12±0.56	5.52±0.38	0.99±0.65

Mean±SD (n=3)

[Pα] and [Pβ]-IAF. For [Pβ]-IAF, cleavage was fastest in the presence of Calu-3, showing a normalized half-life of about 1 h only; in the presence of both HeLa and MDCK cells the half-lives were around 5 h. [Pα] showed the fastest degradation rate, featuring a normalized $t_{1/2}$ value of only 1 h with HeLa and MDCK cells, and 0.5 h with Calu-3 cells.

Identification of Metabolites Emerging from CPP Degradation. To identify the typical cleavage sites of the four investigated CPPs, we analyzed the occurrence of metabolites and identified the resulting fragments of CF-SAP, CF-hCT(9-32)-br, [Pα] and [Pβ]-IAF upon incubation with HeLa, MDCK or Calu-3 cells. Reversed-phase high performance liquid chromatography (RP-HPLC) and matrix assisted laser

desorption ionization time of flight mass spectrometry (MALDI-TOF MS) were used for analysis of the samples. Whereas RP-HPLC revealed the remaining amounts of CPPs and the levels of their metabolites, MALDI-TOF MS allowed us to uncover the identity of N- and C-terminal metabolites (Fig. 4). Using RP-HPLC, only fluorophore-carrying fragments labeled with either N-terminal CF or C-terminal IAF, respectively, were detectable. Because of the insufficient solubility of [Pα]-IAF, [Pα] was exclusively used in its better soluble, unlabeled form. Monitoring was through instrinsic fluorescence based on tryptophan fluorophores and UV. The observed m/z values of the MALDI-TOF mass spectra represent [M+H]+. For control, we analyzed cells incubated with pure medium solution instead of peptide solution. High salt concentrations led to low detection limits and high background noise in MALDI-TOF MS measurements. Introduction of an additional desalting step using ZipTips markedly improved the detection sensitivity. Figure 4 shows two typical MALDI-TOF MS and RP-HPLC spectra, each after 1 and 120 min, and demonstrates that detection of metabolites by MALDI-TOF MS and RP-HPLC was consistent. There was a clear time dependence of degradation. Only few small metabolite peaks emerged after 1 min incubation, whereas several distinct metabolite peaks were observed after 120 min. When incubated with the HeLa, MDCK and Calu-3 cell cultures, each of the four investigated CPPs degraded into between three and ten identifiable metabolites. As shown in
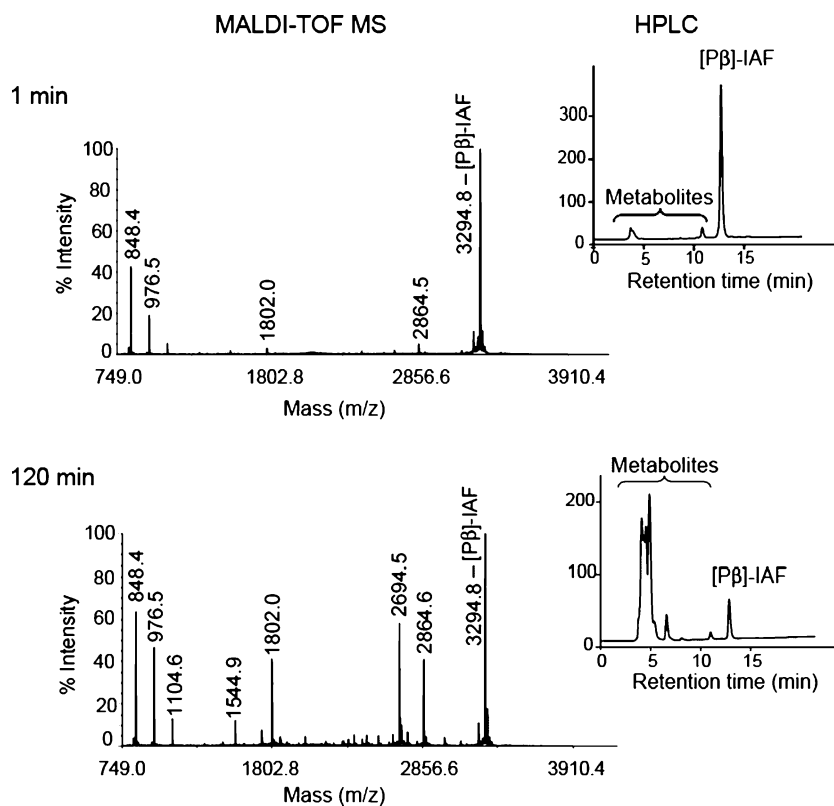
Fig. 4. Typical MALDI-TOF MS and RP-HPLC profiles of metabolites upon metabolic degradation of [Pβ]-IAF in contact with Calu-3 layers. After 1 min, [Pβ]-IAF was practically fully intact and represented by the main peak corresponding to the original CPP in the RP-HPLC diagram as well as in the MALDI-TOF MS spectrum. After 2 h of incubation with Calu-3 cells, the increase in number of metabolite peaks as obtained by RP-HPLC was consistent with that in the MALDI-TOF MS spectra

Fig. 5, all three cell cultures yielded mostly identical metabolite patterns. Due to the high background noise up to 750 Da only fragments above this mass range were considered. A summary of expected and measured molecular weights corresponding to the proposed metabolites is given in Table IV. In these studies, we considered only frequently occurring peptide fragments. These are listed in Table IV, with the main fragments indicated in bold.

Figure 6 schematically illustrates the suggested cleavage patterns of CF-SAP, CF-hCT(9-32)-br, [Pα] and [Pβ]-IAF in contact with either one of the cell cultures. For all peptides, each amino acid (aa) was numbered, including the side chain of CF-hCT(9-32)-br (aa S1–S15).

CF-SAP. We observed only minor cleavage of CF-SAP, in terms of both numbers and peak intensities of the metabolites, corresponding to high stability in contact with HeLa, MDCK and Calu-3 cell cultures over a time interval of 8 h (Table III).

Fig. 5. Identical metabolite patterns of [Pβ]-IAF in all three cell models. MALDI-TOF MS spectra of [Pβ]-IAF after incubation with HeLa, MDCK or Calu-3 cell models, respectively, demonstrate identical metabolite patterns as shown by selected MALDI spectra within the first hour after incubation

Table IV. Measured *Versus* Expected Molecular Weights of Metabolite Fragments Detected by MALDI-TOF MS

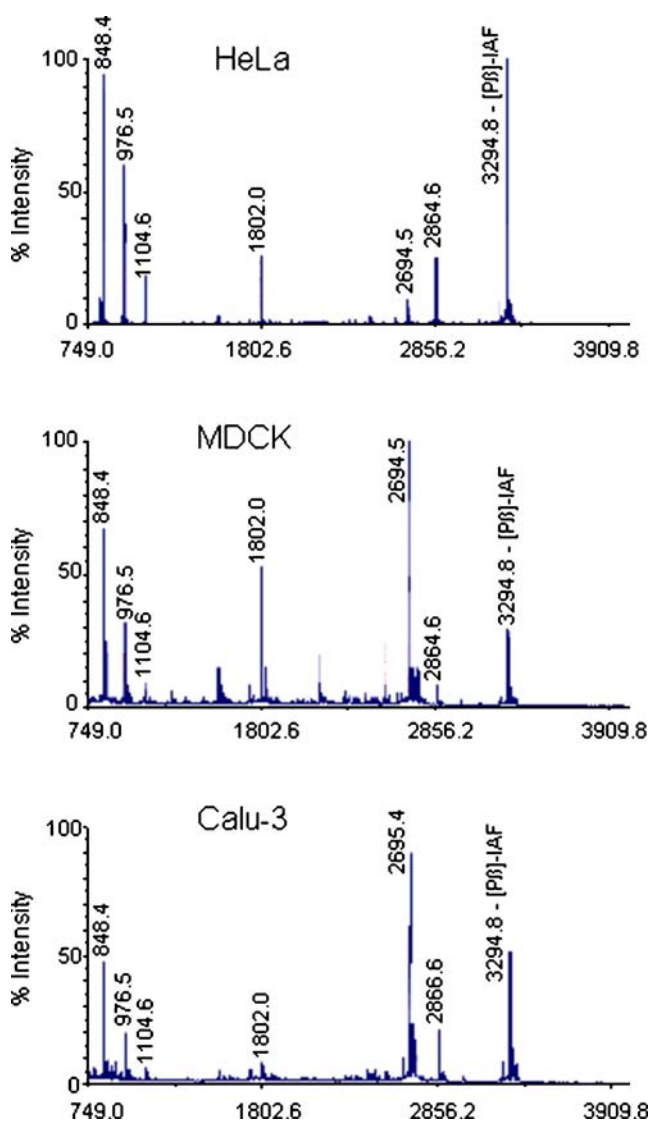| Peptide	Fragment	Measured MW	Calculated MW
CF-SAP	CF-18	2,356.3	2,356.9
	4–18	*1,630.1*	*1,630.3*
	3–13	*1,182.7*	*1,182.7*
CF-hCT(9-32)-br	11–32	3,977.0	3,976.2
	16–25; S14	2,807.6	2,808.8
	17–32	3,322.3	3,322.1
	18–20; S11	1,587.0	1,586.0
	18–22; S5	1,110.4	1,111.0
[Pα]	*10–27*	*1,655.1*	*1,659.2*
	3–14	*1,250.5*	*1,250.7*
	4–23	2,190.2	2,193.9
	6–20	1,577.6	1,580.1
	5–20	1,691.4	1,693.2
[Pβ]-IAF	1-IAF	3,294.8	3,298.2
	5-IAF	2,864.6	2,867.7
	7-IAF	*2,694.5*	*2,697.4*
	17-IAF	*1,802.0*	*1,804.3*
	23-IAF	1,104.6	1,106.4
	24-IAF	976.5	978.2
	25-IAF	*848.4*	*850.0*

Measured and expected MW values represent [M+H]⁺. Metabolites found in all three cell models after approximately 1% to 90% degradation of the CPPs. Most frequently occurring metabolites are indicated in italics. *S* indicates the side chain of CF-hCT(9-32)-br. For all peptides, each amino acid was numbered, including the side chain S1–S15 of CF-hCT(9-32)-br

Nevertheless, some distinct fragments could be revealed, e.g. with cleavage sites within the first trimer between Arg_2 and Leu_3, together with an additional site in the third trimer between Val_{13} and Arg_{14} resulting in the fragment Leu_3-Val_{13} (Table IV and Fig. 6). For this fragment the resulting counterpart, fragment Arg_{14}-Pro_{18}, was also found. A frequently occurring fragment, Pro_4-Pro_{18}, was also found to result from cleavage in the first trimer between Leu_3 and Pro_4.

CF-hCT(9-32)-br. Due to its branched character, the cleavage pattern of CF-hCT(9-32)-br was inherently complex to evaluate. Clear assignments of distinct fragments were difficult and made unequivocal identification problematic. Even more so, the marked stability of this peptide led to weak intensities of metabolite peaks. Hence, for further evaluation we only considered a subset of selected and clearly identifiable fragments. Within the hCT derived backbone of CF-hCT(9-32)-br, the main cleavage sites were between Gly_{10} and Thr_{11}, Asp_{15} and Phe_{16}, and Asn_{17} and Lys_{18}. In the side branch, an important cleavage site was found between Gly_{S5} and Pro_{S6} (Table IV and Fig. 6).

[Pα]. As suggested by its short half-life [Pα] was subject to fast stepwise cleavage of single amino acids from both the C- as well as the N-terminus. Two fragments were observed consistently, namely fragments Ala_{10}-Val_{27} and Leu_3-Leu_{14} indicating distinct cleavage sites between amino acids Leu_3 and Phe_4, Ala_9 and Ala_{10}, and Leu_{14} and Met_{15}. Also we observed cleavage sites in the cationic domain of the molecule at position Lys_{23}-Lys_{24} as well as Lys_{24}-Arg_{25}.

[Pβ]-IAF. Corresponding to their analogous sequences, the degradation patterns of [Pβ]-IAF and [Pα] were similar.

Fig. 6. Scheme of suggested metabolic cleavage sites of CPPs upon incubation with the three cell models. Individually shaded arrowheads correspond to the corresponding cleavage sites between the respective amino acids. The resulting metabolites are indicated through *equally shaded bars* as identified by MALDI-TOF MS

Important cleavage sites were between Gly_6 and Phe_7 as well as between Gly_{16} and Ala_{17} and led to the fragments Phe_7-IAF and Leu_{17}-IAF. As similarly observed for [Pα], one of the peptide's most frequent fragments, Arg_{25}-IAF, was the result of a break in the cationic section between position Lys_{24} and Arg_{25}, suggesting high susceptibility to enzymatic degradation in this domain.

DISCUSSION

The aim of the present study was to investigate the metabolic fate of four CPPs, namely CF-SAP, CF-hCT(9-32)-br, [Pα], and [Pβ]-IAF, when in contact with three selected epithelial cell lines. As yet, information on the subjects of enzymatic stability and degradation of CPPs is rare (10–14). We also studied the cellular translocation efficiency of the four peptides into three epithelial cell cultures. To our knowledge, so far, only few studies scrutinize a relationship between metabolic stability and translocation efficiency of CPPs (37,38).

The metabolic clearance of CPPs has several biomedical aspects: on the one hand, CPPs should be stable enough to deliver a cargo to its destination prior to be metabolically cleared (12). On the other hand, metabolic clearance of CPPs after delivery to its target is desired in order to release the cargo or a biologically active unit thereof, and avoid systemic toxicity.

We investigated the metabolic stability of CF-SAP, CF-hCT(9-32)-br, [Pα], and [Pβ]-IAF in three epithelial cell cultures with different phenotypes and enzymatic activities, namely HeLa, MDCK and Calu-3. On surfaces, HeLa cells grow as proliferating, subconfluent layers with no tight junctional network. By contrast, MDCK cells develop confluent monolayers forming a continuous sheet of cells joined by tight junctions (27). Similarly, the airway epithelial cell line Calu-3 forms polarized and well differentiated monolayers with tight-junctional networks (39) and, different from MDCK, generates extracellular mucus (40,41).

Among the four investigated CPPs, CF-SAP and CF-hCT(9-32)-br were the most stable ones, allowing only minor rates of metabolic cleavage. Even in contact with Calu-3 cells, CF-SAP and CF-hCT(9-32)-br were rather stable whereas the normalized half-lives of intact [Pα] and [Pβ]-IAF were much shorter. We observed higher protein levels per cm^2 for Calu-3 cells as compared to HeLa and MDCK cells. Assuming that protein and enzyme activity levels correlate, we conclude that the increased protein levels in Calu-3 layers contribute to the enhanced metabolism of the four CPPs in this model.

In a former study, we investigated the half-life of the unbranched CF-hCT(9-32) (13). For this linear peptide, a half-life of several hours was found when in contact with MDCK monolayers and less than 1 h with Calu-3 cells. Through side chain modification of CF-hCT(9-32), resulting in the branched CF-hCT(9-32)-br, we achieved not only an

increase in cellular translocation (23) but also improved metabolic stability as shown in the present work. Its improved metabolic stability is concluded to result from efficient steric hindrance through the introduction of the side chain reaching out from K_{18} (Table I). Metabolites of CF-hCT(9-32)-br occurred in only minor quantities as indicated by small peaks in the MALDI-TOF MS spectra. Theoretically, metabolic degradation of the branched CF-hCT(9-32)-br may allow concurrent cleavage in all three segments of the peptide which implies a more complex pattern of theoretically possible fragments as compared to its linear derivative.

Contrasting to the pronounced stability of CF-SAP and CF-hCT(9-32)-br, cleavage of [Pβ]-IAF was rather quick with relatively short half-lives ranging from about 1 h in the presence of Calu-3 cells to about 5 h in the presence of HeLa and MDCK cells. Among the four investigated CPPs, [Pα] had the shortest half-life of around 30 min only. Even in medium alone, i.e. in the absence of any cellular enzyme activity, [Pα] was subject to fast degradation. Possible explanations for its non-enzymatic degradation might be (1) hydrolytic cleavage. Further on, (2) adhesion to cell surfaces and/or working material (42) and (3) exclusion from analytical detection by insufficient solubility and aggregation may occur. In fact, we observed high affinity of [Pα]-IAF to membrane surfaces. The limited solubilities and aggregation potential of [Pα]-IAF and [Pβ]-IAF have to be taken into account for the interpretation of results from uptake and metabolism studies. Therefore, to avoid misinterpretations, we focus on the individual relationship of uptake efficiency and metabolism of each peptide in cultures of the three cell lines, rather than comparing between the peptides. Structural differences between [Pβ]-IAF and [Pα] through amino acid modifications of Gly_6, Gly_9, Gly_{12}, Thr_{14} and Ala_{17} *versus* Ala_6, Ala_9, Leu_{12}, Leu_{14} and Leu_{17}, respectively, were of no significant impact on the net chemical stability of the peptides as indicated by the occurrence of the cleavage sites Gly_6-Phe_7 and Gly_{16}-Ala_{17} for [Pβ]-IAF, *versus* Ala_9-Ala_{10} and Leu_{14}-Met_{15} for [Pα]. Furthermore, there was no reduction in the number of cleavage sites through these modifications. Equally, the sequence modifications did not have any significant effect on the efficiency of translocation of these two CPPs in the investigated cell lines. Altogether, in spite of differences in extent, there was no major difference in the cleavage patterns between the three cell lines for each of the investigated CPPs. This finding is in good agreement with a former study of our group where we described similar cleavage patterns for hCT derived CPPs irrespective of the applied epithelial cell model (13).

In order to assess the impact of metabolic cleavage on the efficiency of translocation, we tried to estimate the extent of translocation of CF-SAP, CF-hCT(9-32)-br, [Pα]-IAF and [Pβ]-IAF. For all investigated CPPs, we observed efficient uptake in HeLa cells by CLSM and FACS. Corresponding to its higher state of cellular differentiation, uptake in the MDCK model was significantly reduced for each of the four CPPs, and none of the CPPs was observed to translocate efficiently into confluent Calu-3 cells. Hallbrink *et al.* (14) recently suggested that the uptake of cell-penetrating peptides is dependent on the peptide-to-cell ratio. As a consideration of the lack of uptake in MDCK and Calu cells, there is a relatively much higher number of cells in these experiments as compared with the uptake in HeLa.

Owing to the poor aqueous solubility of the IAF-labeled [Pα]-IAF, we analyzed its metabolism kinetics with unlabeled [Pα] which was sufficiently soluble. Obviously, this prohibits from a direct extrapolation of data from [Pα] to [Pα]-IAF. However, for FACS and CLSM, which required more sensitive fluorescence detection, we used [Pα]-IAF expecting translocation to occur with the available fraction of dissolved peptide only.

CONCLUSION

We demonstrate in the present study that CPP stability and translocation capacity were strongly cell line dependent, whereas their cleavage patterns were quite similar between the three cell cultures. When comparing all four CPPs, there was no direct relation between metabolic stability and translocation efficiency indicating that stability is not the main limiting factor in cellular translocation, at least in the investigated cell cultures. However, in the context of individual CPPs, stabilization against chemical as well as enzymatic degradation may further improve their translocation efficiency. For this purpose, enhanced metabolic CPP stability may be achieved through replacement of L-amino acids by their non-physiologic D-counterparts, through N-methylation or exchange of certain amino acids.

ACKNOWLEDGMENTS

REFERENCES

1. L. A. Kueltzo, and C. R. Middaugh. Potential use of non-classical pathways for the transport of macromolecular drugs. *Expert Opin. Investig. Drugs*. **9**:2039–2050 (2000).
2. D. Derossi, A. H. Joliot, G. Chassaing, and A. Prochiantz. The third helix of the Antennapedia homeodomain translocates through biological membranes. *J. Biol. Chem*. **269**:10444–10450 (1994).
3. E. Vives, P. Brodin, and B. Lebleu. A truncated HIV-1 Tat protein basic domain rapidly translocates through the plasma membrane and accumulates in the cell nucleus. *J. Biol. Chem*. **272**:16010–16017 (1997).
4. A. Prochiantz. Getting hydrophilic compounds into cells: lessons from homeopeptides. *Curr. Opin. Neurobiol*. **6**:629–634 (1996).
5. S. R. Schwarze, A. Ho, A. Vocero-Akbani, and S. F. Dowdy. *In vivo* protein transduction: delivery of a biologically active protein into the mouse. *Science*. **285**:1569–1572 (1999).
6. D. Singh, S. K. Bisland, K. Kawamura, and J. Gariepy. Peptide-based intracellular shuttle able to facilitate gene transfer in mammalian cells. *Bioconjug. Chem*. **10**:745–754 (1999).
7. M. Lewin, N. Carlesso C. H. Tung *et al.* Tat peptide-derivatized magnetic nanoparticles allow *in vivo* tracking and recovery of progenitor cells. *Nat. Biotechnol*. **18**:410–414 (2000).
8. A. Astriab-Fisher, D. Sergueev, M. Fisher, B. R. Shaw, and R. L. Juliano. Conjugates of antisense oligonucleotides with the Tat

and antennapedia cell-penetrating peptides: effects on cellular uptake, binding to target sequences, and biologic actions. *Pharm. Res*. **19**:744–754 (2002).

9. J. A. Fix. Oral controlled release technology for peptides: status and future prospects. *Pharm. Res*. **13**:1760–1764 (1996).
10. R. Fischer, K. Kohler, M. Fotin-Mleczek, and R. Brock. A stepwise dissection of the intracellular fate of cationic cell-penetrating peptides. *J. Biol. Chem*. **279**:12625–12635 (2004).
11. A. Elmquist, M. Lindgren, T. Bartfai, and U. Langel. VE-cadherin-derived cell-penetrating peptide, pVEC, with carrier functions. *Exp. Cell. Res*. **269**:237–244 (2001).
12. A. Elmquist, and U. Langel. *In vitro* uptake and stability study of pVEC and its all-D analog. *Biol. Chem*. **384**:387–393 (2003).
13. R. Trehin, H. M. Nielsen, H. G. Jahnke, U. Krauss, A. G. Beck-Sickinger, and H. P. Merkle. Metabolic cleavage of cell-penetrating peptides in contact with epithelial models: human calcitonin (hCT)-derived peptides, Tat(47-57) and penetratin(43-58). *Biochem. J*. **382**:945–956 (2004).
14. M. E. Lindgren, M. M. Hallbrink, A. M. Elmquist, and U. Langel. Passage of cell-penetrating peptides across a human epithelial cell layer *in vitro. Biochem. J*. **377**:69–76 (2004).
15. G. Karp. Cell and molecular biology, 2nd edn, John Wiley & Sons, New York, 1999.
16. K. Simons, and S. D. Fuller. Cell surface polarity in epithelia. *Annu. Rev. Cell Biol*. **1**:243–288 (1985).
17. B. I. Florea, M. L. Cassara, H. E. Junginger, and G. Borchard. Drug transport and metabolism characteristics of the human airway epithelial cell line Calu-3. *J. Control Release*. **87**:131–138 (2003).
18. L. Crespo, G. Sanclimens B. Montaner *et al*. Peptide dendrimers based on polyproline helices. *J. Am. Chem. Soc*. **124**:8876–8883 (2002).
19. J. Fernandez-Carneado, M. J. Kogan, S. Castel, and E. Giralt. Potential peptide carriers: amphipathic proline-rich peptides derived from the N-terminal domain of gamma-Zein. *Angew. Chem. Int. Ed. Engl*. **43**:1811–1814 (2004).
20. J. Fernandez-Carneado, M. J. Kogan, S. Pujals, and E. Giralt. Amphipathic peptides and drug delivery. *Biopolymers*. **76**:196–203 (2004).
21. R. Trehin, U. Krauss, R. Muff, M. Meinecke, A. G. Beck-Sickinger, and H. P. Merkle. Cellular internalization of human calcitonin derived peptides in MDCK monolayers: a comparative study with Tat(47-57) and penetratin(43-58). *Pharm. Res*. **21**:33–42 (2004).
22. U. Krauss, M. Muller, M. Stahl, and A. G. Beck-Sickinger. *In vitro* gene delivery by a novel human calcitonin (hCT)-derived carrier peptide. *Bioorg. Med. Chem. Lett*. **14**:51–54 (2004).
23. C. Foerg, U. Ziegler J. Fernandez-Carneado *et al*. Decoding the entry of two novel cell-penetrating peptides in HeLa Cells: lipid Raft-mediated endocytosis and endosomal escape. *Biochemistry*. **44**:72–81 (2005).
24. P. Vidal, M. C. Morris, L. Chaloin, J. Mery, F. Heitz, and G. Divita. Conformations of a synthetic peptide which facilitates the cellular delivery of nucleic acids. *Lett. Pept. Sci*. **4**:227–230 (1997).
25. M. C. Morris, P. Vidal, L. Chaloin, F. Heitz, and G. Divita. A new peptide vector for efficient delivery of oligonucleotides into mammalian cells. *Nucleic Acids Res*. **25**:2730–2736 (1997).
26. S. Deshayes, T. Plenat, G. Aldrian-Herrada, G. Divita, C. Le Grimellec, and F. Heitz. Primary amphipathic cell-penetrating

peptides: structural requirements and interactions with model membranes. *Biochemistry*. **43**:7698–7706 (2004).
27. B. Rothen-Rutishauser, S. D. Kramer, A. Braun, M. Gunthert, and H. Wunderli-Allenspach. MDCK cell cultures as an epithelial *in vitro* model: cytoskeleton and tight junctions as indicators for the definition of age-related stages by confocal microscopy. *Pharm. Res*. **15**:964–971 (1998).
28. M. C. Morris, V. Robert-Hebmann L. Chaloin *et al*. A new potent HIV-1 reverse transcriptase inhibitor. A synthetic peptide derived from the interface subunit domains. *J. Biol. Chem*. **274**:24941–24946 (1999).
29. J. P. Richard, K. Melikov E. Vives *et al*. Cell-penetrating peptides. A reevaluation of the mechanism of cellular uptake. *J. Biol. Chem*. **278**:585–590 (2003).
30. S. Sahlin, J. Hed, and I. Rundquist. Differentiation between attached and ingested immune-complexes by a fluorescence quenching cytofluorometric assay. *J. Immunol. Methods*. **60**:115–124 (1983).
31. Z. S. Ma, and L. Y. Lim. Uptake of chitosan and associated insulin in Caco-2 cell monolayers: A comparison between chitosan molecules and chitosan nanoparticles. *Pharm. Res*. **20**:1812–1819 (2003).
32. C. P. Wan, C. S. Park, and B. H. S. Lau. A rapid and simple microfluorometric phagocytosis assay. *J. Immunol. Methods*. **162**:1–7 (1993).
33. W. C. Tseng, N. B. Purvis, F. R. Haselton, and T. D. Giorgio. Cationic liposomal delivery of plasmid to endothelial cells measured by quantitative flow cytometry. *Biotechnol. Bioeng*. **50**:548–554 (1996).
34. J. Hed, G. Hallden, S. G. Johansson, and P. Larsson. The use of fluorescence quenching in flow cytofluorometry to measure the attachment and ingestion phases in phagocytosis in peripheral blood without prior cell separation. *J. Immunol. Methods*. **101**:119–125 (1987).
35. N. P. Innes, and G. R. Ogden. A technique for the study of endocytosis in human oral epithelial cells. *Arch. Oral Biol*. **44**:519–523 (1999).
36. H. C. Kang, Y. H. Park, and S. J. Go. Growth inhibition of a phytopathogenic fungus, *Colletotrichum* species by acetic acid. *Microbiol. Res*. **158**:321–326 (2003).
37. D. S. Youngblood, S. A. Hatlevig, J. N. Hassinger, P. L. Iversen, and H. M. Moulton. Stability of cell-penetrating peptide-morpholino oligomer conjugates in human serum and in cells. *Bioconjug. Chem*. **18**:50–60 (2007).
38. C. Palm, M. Jayamanne, M. Kjellander, and M. Hallbrink. Peptide degradation is a critical determinant for cell-penetrating peptide uptake. *Biochim. Biophys. Acta*. **1768**:1769–1776 (2007).
39. B. Q. Shen, W. E. Finkbeiner, J. J. Wine, R. J. Mrsny, and J. H. Widdicombe. Calu-3: a human airway epithelial cell line that shows cAMP-dependent Cl- secretion. *Am. J. Physiol*. **266**:L493–501 (1994).
40. I. I. Forbes. Human airway epithelial cell lines for *in vitro* drug transport and metabolism studies. *Pharm. Sci. Technol. Today*. **3**:18–27 (2000).
41. N. R. Mathia, J. Timoszyk, P. I. Stetsko, J. R. Megill, R. L. Smith, and D. A. Wall. Permeability characteristics of calu-3 human bronchial epithelial cells: *in vitro-in vivo* correlation to predict lung absorption in rats. *J. Drug Target*. **10**:31–40 (2002).
42. D. E. Chico, R. L. Given, and B. T. Miller. Binding of cationic cell-permeable peptides to plastic and glass. *Peptides*. **24**:3–9 (2003).